Biophysical Journal, Volume *114*

Supplemental Information

Coexistence and Pattern Formation in Bacterial Mixtures with Contact-Dependent Killing

Liyang Xiong, Robert Cooper, and Lev S. Tsimring

Supporting Material
Coexistence and pattern formation in bacterial mixtures with contact-dependent killing and long-range inhibition

Liyang Xiong,[1,2] Robert Cooper,[2] and Lev S. Tsimring[2,3]

[1] *Department of Physics, University of California, San Diego, La Jolla, California, USA*
[2] *BioCircuits Institute, University of California, San Diego, La Jolla, California, USA*
[3] *The San Diego Center for Systems Biology, UCSD, La Jolla, CA, USA*

I. ANALYSIS OF THE TWO-STRAIN MODEL

We consider the interaction of two strains of bacteria, fast-growing strain 1 with local density $n_1(\mathbf{r},t) and slow-growing strain 2 with local density n_2(\mathbf{r},t)$. The growth of both strains is limited by the total local density of bacteria, so when n_1+n_2 approaches n_0, the growth of both strains saturates. Both strains are characterized by the same death rate δ. Additionally, strain 2 kills strain 1 on direct contact with the rate κ. Both strains are assumed to diffuse horizontally with the same small diffusion constant D_n. The model reads as follows

$$\frac{\partial n_1}{\partial t} = \gamma_1 n_1(1-\frac{n_1+n_2}{n_0}) - \delta n_1 - \kappa n_1 n_2 + D_n\nabla^2 n_1 \tag{S1}$$

$$\frac{\partial n_2}{\partial t} = \gamma_2 n_2(1-\frac{n_1+n_2}{n_0}) - \delta n_2 + D_n\nabla^2 n_2 \tag{S2}$$

In the following, we assume that all parameters $\gamma_1,\gamma_2,\delta,\kappa,D_n,n_0$ are positive. Without loss of generality, we can rescale time $\tilde{t}=\gamma_2 t$, space $\tilde{x}=(\gamma_2/D_n)^{1/2}x$, and densities, $\tilde{n}=n/n_0$, so in rescaled variables $\tilde{\gamma}_2=1,\tilde{\gamma}_1=\gamma_1/\gamma_2,\tilde{\delta}=\delta/\gamma_2,\tilde{\kappa}=\kappa n_0/\gamma_2,\tilde{D}_n=1$. For simplicity, in the following we will drop tildas and keep the same notation for the rescaled variables and parameters:

$$\frac{\partial n_1}{\partial t} = \gamma_1 n_1(1-n_1-n_2) - \delta n_1 - \kappa n_1 n_2 + \nabla^2 n_1 \tag{S3}$$

$$\frac{\partial n_2}{\partial t} = n_2(1-n_1-n_2) - \delta n_2 + \nabla^2 n_2 \tag{S4}$$

Spatially uniform steady states and their stability. This system has four steady states:

1. $n_1 = 1-\frac{\delta}{\gamma_1}, n_2 = 0$.
2. $n_1 = 0$, $n_2 = 1-\delta$.
3. $n_1 = 1-\delta-\frac{\delta}{\kappa}(\gamma_1-1)$, $n_2 = \frac{\delta}{\kappa}(\gamma_1-1)$.
4. $n_1 = n_2 = 0$.

The Jacobian matrix is

$$J = \begin{pmatrix} a_{11} & a_{12} \\ a_{21} & a_{22} \end{pmatrix}$$

with

$$a_{11} = \gamma_1(1-2n_1-n_2) - \delta - \kappa n_2 \tag{S5}$$

$$a_{12} = -\gamma_1 n_1 - \kappa n_1 \tag{S6}$$

$$a_{21} = -n_2 \tag{S7}$$

$$a_{22} = 1-n_1-2n_2-\delta \tag{S8}$$

Steady state 1 has eigenvalues $\lambda_1=\delta-\gamma_1, \lambda_2=(\frac{1}{\gamma_1}-1)\delta$. When $\gamma_1>\delta,1$, it is stable and $n_1>0$. Steady state 2 has eigenvalues $\lambda_1=(\gamma_1-1)\delta-\kappa(1-\delta), \lambda_2=\delta-1$. When $\delta<1$ and $\kappa>\kappa_b=\frac{\delta(\gamma_1-1)}{1-\delta}$, it is stable and $n_2>0$. Steady state 3 is positive when $\gamma_1>1$, $\delta<1$ and $\kappa>\kappa_b$ but is unstable. Trivial steady state 4 is unstable if $\gamma_1>\delta$ or $\delta<1$.

The system is bistable in the range

$$1 < \gamma_1 < 1 + \frac{\kappa(1-\delta)}{\delta} \tag{S9}$$

Stationary front in two-variable model. In the bistable regime, there may exist fronts separating colonies of strains 1 and 2. These fronts generally move in either direction depending on the system parameters. Generally, if $\gamma_1 > 1$, for very small killing rate κ, strain 1 always wins, and the front propagates in the direction of strain 2, while for sufficiently large κ the front reverses. There is a unique value of $\kappa_s = \kappa(\gamma_1, \delta)$ at which the front is stationary. This value of κ_s can be found approximately for small δ and κ, when $n_1 + n_2$ is close to 1 using the Maxwell rule known in thermodynamics.

In the following we assume that $\kappa = \epsilon K$, $\delta = \epsilon\Delta$ with $\epsilon \ll 1$, and introduce new variables

$$N = \epsilon^{-1}(n_1 + n_2 - 1), \quad \xi = n_1 - n_2. \tag{S10}$$

Conversely, $n_1 = (1 + \epsilon N + \xi)/2, n_2 = (1 + \epsilon N - \xi)/2$. In the new variables and in the first order in ϵ, Eqs. (S3),(S4) can be rewritten as

$$\partial_t N = -\frac{N}{2}(\gamma_1 + 1) - \frac{N}{2}(\gamma_1 - 1)\xi - \Delta - \frac{K}{4}(1 - \xi^2) + \nabla^2 N, \tag{S11}$$

$$\epsilon^{-1}\partial_t \xi = -\frac{N}{2}(\gamma_1 - 1) - \frac{N}{2}(\gamma_1 + 1)\xi - \Delta\xi - \frac{K}{4}(1 - \xi^2) + \epsilon^{-1}\nabla^2\xi. \tag{S12}$$

The first equation describes fast relaxation toward the solution

$$N = -\frac{2\left(\Delta + \frac{K}{4}(1 - \xi^2)\right)}{\gamma_1 + 1 + \xi(\gamma_1 - 1)}. \tag{S13}$$

Assuming that the fast initial relaxation has occurred, and N is slaved to slow variably ξ, we can substitute N from Eq. (S13) in Eq. (S12). Returning to the original parameters κ and δ, after simple algebra we get a single reaction-diffusion equation for the slow dynamics of ξ,

$$\partial_t \xi = f(\xi) + \nabla^2 \xi, \tag{S14}$$

where

$$f(\xi) = \delta \frac{1 - \xi^2}{1 + \Gamma\xi}\left[\Gamma + (\Gamma - 1)(1 - \xi)\frac{\kappa}{4\delta}\right] \tag{S15}$$

with $\Gamma = (\gamma_1 - 1)/(\gamma_1 + 1)$. For small δ and κ, this equation describes slow front propagation. Function $f(\xi)$ has two roots $\xi_{1,2} = \pm 1$ corresponding to stable fixed points of Eq. (S14), and an intermediate root at $\Gamma + (\Gamma - 1)(1 - \xi)\frac{\kappa}{4\delta} = 0$ corresponding to an unstable fixed point. Maxwell rule states that a front solution of the 1-D reaction-diffusion equation (S14) connecting stable fixed points ξ_1 and ξ_2 is stationary if $\int_{\xi_1}^{\xi_2} f(\xi) d\xi = 0$.

For $\Gamma \ll 1$, we can drop $\Gamma\xi$ in the denominator of (S15). Then it becomes a cubic polynomial, and it is evident that the integral will be zero if $f(\xi)$ is anti-symmetric with respect to zero, i.e. when intermediate root is $\xi = 0$, or $\Gamma + (\Gamma - 1)\frac{\kappa}{4\delta} = 0$, which gives

$$\frac{\kappa}{\delta} = 2(\gamma_1 - 1). \tag{S16}$$

For finite Γ, integration of the full function (S15) yields the following expression for the ratio κ/δ at which the front is stationary,

$$\frac{\kappa}{\delta} = \frac{3(\gamma_1 - 1)^2(\gamma_1^2 - 1 - 2\gamma_1 \ln \gamma_1)}{2\gamma_1^3 + 3\gamma_1^2 - 6\gamma_1 + 1 - 6\gamma_1^2 \ln \gamma_1}. \tag{S17}$$

It is easy to check that expression (S17) reduces to (S16) for small $\gamma_1 - 1$.

II. ANALYSIS OF THE THREE-VARIABLE MODEL

The full model with long-range inhibition reads as follows

$$\frac{\partial n_1}{\partial t} = \frac{\gamma_1}{1+A/A_0} n_1 \left(1 - \frac{n_1+n_2}{n_0}\right) - \delta n_1 - \kappa n_1 n_2 + D_n \nabla^2 n_1, \tag{S18}$$

$$\frac{\partial n_2}{\partial t} = \gamma_2 n_2 \left(1 - \frac{n_1+n_2}{n_0}\right) - \delta n_2 + D_n \nabla^2 n_2, \tag{S19}$$

$$\frac{\partial A}{\partial t} = \gamma_A n_1 - \delta_A A + D_A \nabla^2 A. \tag{S20}$$

Use the same scaling as above and $\tilde{A} = A/A_0, \tilde{\gamma}_A = \gamma_A n_0/(\gamma_2 A_0), \tilde{\delta}_A = \delta_A/\gamma_2, \tilde{D}_A = D_A/D_n$, we have

$$\frac{\partial n_1}{\partial t} = \frac{\gamma_1}{1+A} n_1(1-n_1-n_2) - \delta n_1 - \kappa n_1 n_2 + \nabla^2 n_1 \tag{S21}$$

$$\frac{\partial n_2}{\partial t} = n_2(1-n_1-n_2) - \delta n_2 + \nabla^2 n_2 \tag{S22}$$

$$\frac{\partial A}{\partial t} = \gamma_A n_1 - \delta_A A + D_A \nabla^2 A \tag{S23}$$

where we again drop tildes for simplicity of notation.

Bifurcation analysis of the spatially uniform steady states. Full three-variable system possesses at most 5 real spatially uniform steady states:

1. $n_1 = \frac{\gamma_1-\delta}{\frac{\delta\gamma_A}{\delta_A}+\gamma_1}, n_2 = 0, A = \frac{\gamma_1-\delta}{\delta+\frac{\gamma_1\delta_A}{\gamma_A}}$.
2. $n_1 = 0, n_2 = 1-\delta, A = 0$.
3. $n_1 = \frac{-b+\sqrt{b^2-4ac}}{2a}, n_2 = 1-n_1-\delta, A = \frac{\gamma_A}{\delta_A} n_1$ where $a = \frac{\kappa\gamma_A}{\delta_A}, b = \kappa - \frac{\gamma_A}{\delta_A}[\delta + \kappa(1-\delta)], c = (\gamma_1-1)\delta - \kappa(1-\delta)$.
4. $n_1 = \frac{-b-\sqrt{b^2-4ac}}{2a}, n_2 = 1-n_1-\delta, A = \frac{\gamma_A}{\delta_A} n_1$ where a, b, c are the same as those in steady state 3.
5. $n_1 = 0, n_2 = 0, A = 0$.

The Jacobian matrix for the system is

$$J = \begin{pmatrix} a_{11} & a_{12} & a_{13} \\ a_{21} & a_{22} & a_{23} \\ a_{31} & a_{32} & a_{33} \end{pmatrix}$$

with

$$\begin{aligned} a_{11} &= \frac{\gamma_1}{1+A}(1-2n_1-n_2) - \delta - \kappa n_2 \\ a_{12} &= -\frac{\gamma_1}{1+A} n_1 - \kappa n_1 \\ a_{13} &= -\frac{\gamma_1}{(1+A)^2} n_1(1-n_1-n_2) \\ a_{21} &= -n_2 \\ a_{22} &= 1-n_1-2n_2-\delta \\ a_{23} &= 0 \\ a_{31} &= \gamma_A \\ a_{32} &= 0 \\ a_{33} &= -\delta_A. \end{aligned}$$

The trivial fixed point 5 is always unstable, and we will not consider it below. The steady states of n_1, n_2 vs. κ with their stability are illustrated in Fig. S1(A),(B). When γ_1 is smaller than a threshold γ_{1c}, steady states 3 and 4 always exist although steady state 3 is non-physical in this case (it corresponds to negative n_2) [Fig. S1(C) left]. At the critical value $\gamma_1 = \gamma_{1c}$, a codimension-2 bifurcation occurs when steady state 2 overlaps with steady states

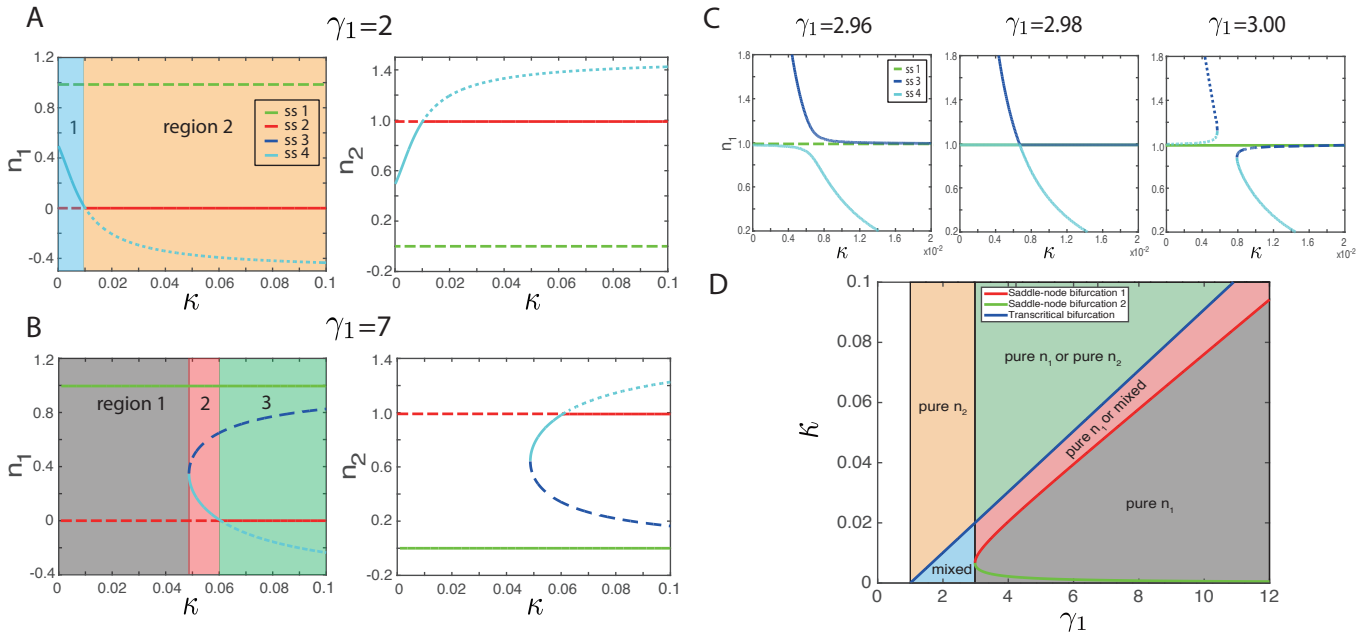

FIG. S1: (A),(B) Steady states of n_1 and n_2 for different γ_1 and κ. Solid lines correspond to stable solutions, long-dashed to unstable solutions, and short-dashed to non-physical steady states for which either n_1 or n_2 are negative. (C) Codimension-2 bifurcation at $\gamma_{1c} = 2.98$. when two saddle-node bifurcation points are born at certain γ_1 and κ and pure solution $n_1 \neq 0, n_2 = 0$ changes stability. (D) Domains of different stable steady states in the (γ_1, κ) parameter plane. Other parameters: $\delta = 0.01, \gamma_A = 0.04, \delta_A = 0.02$.

3 and 4 and two saddle-node bifurcation points emerge [Fig. S1(C) middle]. When $\gamma_1 > \gamma_{1c}$, there are two isolated saddle-node bifurcation points in which steady states 3 and 4 merge and disappear [Fig. S1(C) right].

The condition for the saddle-node bifurcation is $b^2 - 4ac = 0$, which leads to the equation for bifurcation values of $\kappa = \kappa_s$,

$$[1 + \frac{\gamma_A}{\delta_A}(1-\delta)]^2\kappa_s^2 - 2\frac{\gamma_A\delta}{\delta_A}[2\gamma_1 - 1 - \frac{\gamma_A}{\delta_A}(1-\delta)]\kappa_s + \left(\frac{\gamma_A\delta}{\delta_A}\right)^2 = 0, \tag{S24}$$

and thus

$$\kappa_{s\pm} = \frac{\gamma_A\delta}{\delta_A}\left\{\frac{2\gamma_1 - 1 - \frac{\gamma_A}{\delta_A}(1-\delta) \pm 2\sqrt{\gamma_1^2 - \gamma_1[1 + \frac{\gamma_A}{\delta_A}(1-\delta)]}}{[1 + \frac{\gamma_A}{\delta_A}(1-\delta)]^2}\right\}. \tag{S25}$$

From Eq. (S25), it can be shown that $\kappa_{s\pm}$ are real only when

$$\gamma_1 > \gamma_{1c} = 1 + \frac{\gamma_A}{\delta_A}(1-\delta). \tag{S26}$$

We also notice that there is a transcritical bifurcation between steady states 2 and 4 [Fig. S1(A)(B)]. At the transcritical bifurcation point, $n_1 = 0$ which leads to $c = 0$, and thus

$$\kappa = \kappa_t = \frac{\delta(\gamma_1 - 1)}{1 - \delta}. \tag{S27}$$

It is worth mentioning that if $b > 0$ at $\kappa = \kappa_{s_+}$, the saddle-node bifurcation between steady states 3 and 4 happens at $n_1 < 0$, and then the transcritical bifurcation occurs between steady states 2 and 3 instead of 2 and 4 (an example is shown in Fig. S2). In this case, region 2 in Fig. S1(B) disappears, and only regions 1 and 3 remain.

Domains in the parameter plane (γ_1, κ) corresponding to different spatially-uniform stable steady states are shown in Fig. S1(D).

Localized spot of n_1. Here we find an approximate solution for the width of a stationary spot of n_1 surrounded by the sea of n_2, when the diffusion coefficient of A is large but finite. For that we need to compute the distribution

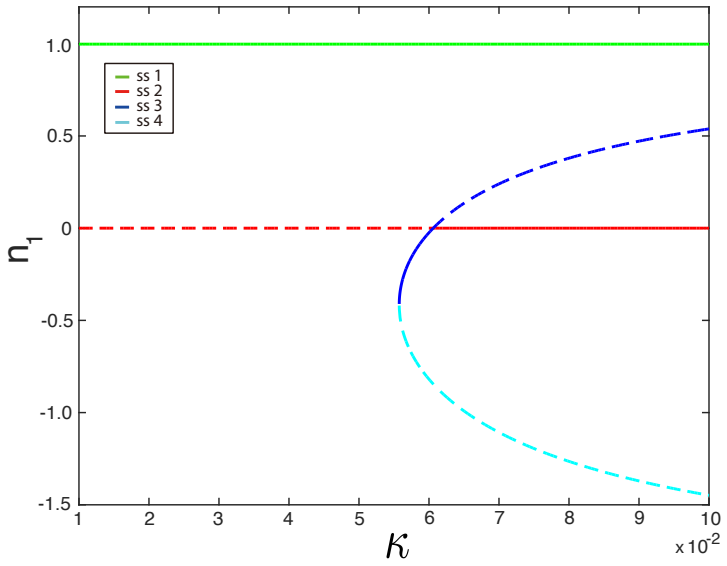

FIG. S2: For sufficiently large γ_1 and small γ_A, the saddle-node bifurcation between steady states 3 and 4 moves to (non-physical) negative n_1, and the transcritical bifurcation occurs between steady states 2 and 3. Parameters: $\gamma_1 = 7, \gamma_A = 0.01$, other parameters are the same as in Fig. S1.

of A produced by such a spot, and find at which spot size the level of A within the spot is such that the interfaces between n_1 and n_2 are stationary. To compute the stationary distribution of A we use Eq. (S23) with $\partial_t A = 0$,

$$\gamma_A n_1 - \delta_A A + D_A \nabla^2 A = 0. \tag{S28}$$

We consider only the 1D case here, but the generalization to 2D is straightforward. We assume that the spot size is much larger than the width of the interfaces separating n_1 and n_2 (which is of the order of $(D_n/\gamma_1)^{1/2}$), but much smaller than the diffusive scale of the inhibitor $q = (\delta_A/D_A)^{1/2}$, and so the spot can be approximated by a rectangular "pulse" with constant $n_1 \approx n_{1*} = 1 - \delta(1 + A(0))/\gamma_1$ for $-x_0 < x < x_0$ and zero outside (see Fig. 3A of the Main text). Solving the Poisson equation (S28) in these two domains and matching A and dA/dx at $x = \pm x_0$, we obtain the following solution for $A(x)$:

$$A(x) = \begin{cases} \frac{\gamma_A}{\delta_A} n_{1*}(1 - e^{-qx_0}\cosh(qx)), & -x_0 < x < x_0 \\ \frac{\gamma_A}{\delta_A} n_{1*} \frac{e^{qx_0} - e^{-qx_0}}{2} e^{-q|x|}, & |x| > x_0 \end{cases} \tag{S29}$$

Substituting $n_{1*} = 1 - \delta(1 + A(0))/\gamma_1$ in Eq. (S29) and take $x = 0$, we can obtain $A(0)$ explicitly,

$$A(0) = \frac{\frac{\gamma_A}{\delta_A}\left(1 - \frac{\delta}{\gamma_1}\right)(1 - e^{-qx_0})}{1 + \frac{\gamma_A \delta}{\gamma_1 \delta_A}(1 - e^{-qx_0})} \tag{S30}$$

The value of A at the front is

$$A(x_0) = \frac{\frac{\gamma_A}{\delta_A}\left(1 - \frac{\delta}{\gamma_1}\right)(1 - e^{-qx_0}\cosh(qx_0))}{1 + \frac{\gamma_A \delta}{\gamma_1 \delta_A}(1 - e^{-qx_0})} \tag{S31}$$

For large inhibitor diffusion, $qx_0 \ll 1$, the difference between $A(0)$ and $A(x_0)$ is small, these expressions can be further simplified to

$$A(0) \approx A(x_0) \approx \frac{\gamma_A}{\delta_A}\left(1 - \frac{\delta}{\gamma_1}\right) qx_0, \tag{S32}$$

which shows that for small x_0 the magnitude of A bump is proportional to x_0, as expected. The spot will be neither expanding nor shrinking if the value of $\gamma_1^* = \gamma_1/(1 + A(x_0))$ with $A(x_0)$ from (S31) satisfies Eq. (S17), which yields the equation for x_0.

Turing-like instability. To explore the possibility of a linear Turing-like instability in our three-component system, we linearized Eqs. (S21)-(S23) near relevant fixed points and studied the eigenvalues corresponding to spatially-periodic perturbations $\sim \exp(ikx + \lambda t)$. Each fixed point has three eigenvalues. Fig. S3 shows three examples of maximal eigenvalues of relevant steady states in different parameter regions [regions 1, 2 and 3 in Fig. S1(B)] vs. wave number k. The middle panel ($\kappa = 0.053$) indeed demonstrates the occurrence of the Turing-like instability when steady state 4 is unstable with respect to small perturbations within a finite range of wavenumbers. The right panel ($\kappa = 0.07$) shows the situation when the fixed point is unstable with respect to spatially uniform as well as spatially-periodic perturbations, but the maximal growth rate occurs at a finite wavenumber. Our numerical simulations show that stable patterns are also possible in this parameter range.

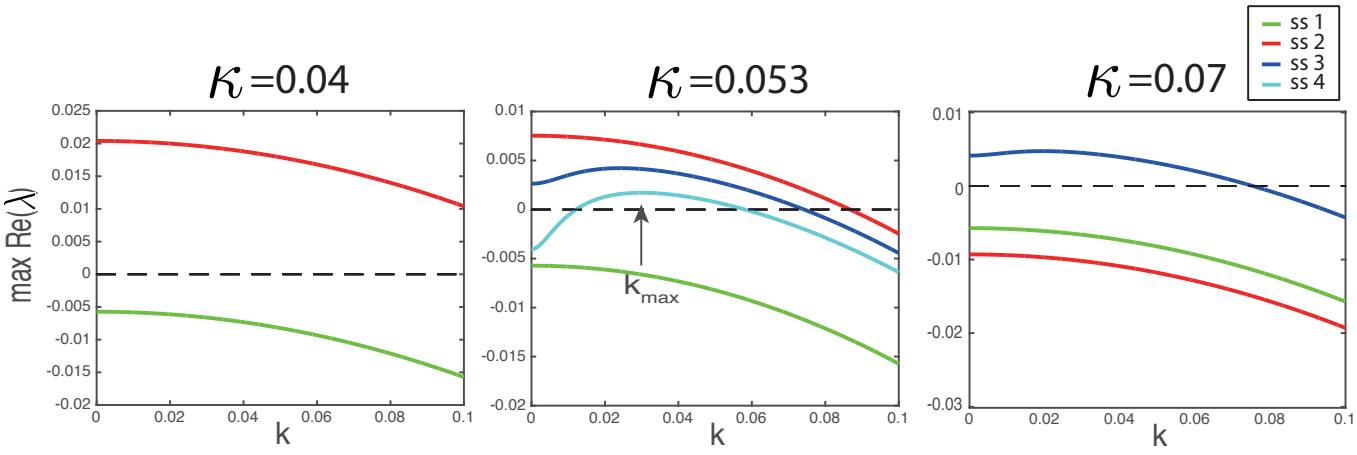

FIG. S3: Maximal real parts of eigenvalues of different steady states in different regions (regions 1, 2 and 3) in Fig. S1(B) vs. wave number k. Parameters are $\gamma_1 = 7, \delta = 0.01, \gamma_A = 0.04, \delta_A = 0.02, D_A = 100$.

III. DUAL-INHIBITION MODEL

To formulate the model considered in the Main text, we assumed that the long-range inhibitor A was only produced by the T6SS-sensitive strain, and only affected its own growth. To generalize this model, here we assume that A is produced by both n_1 and n_2 and it also can inhibit the growth rates of both strains, although not necessarily equally. Furthermore, here we allow strains to have different death rates δ_1 and δ_2. We still assume that both strains have the same diffusion constant for simplicity. Now the model equations read as

$$\frac{\partial n_1}{\partial t} = \frac{\gamma_1}{1+A} n_1(1 - n_1 - n_2) - \delta_1 n_1 - \kappa n_1 n_2 + \nabla^2 n_1, \tag{S33}$$

$$\frac{\partial n_2}{\partial t} = \frac{1}{1+\alpha A} n_2(1 - n_1 - n_2) - \delta_2 n_2 + \nabla^2 n_2, \tag{S34}$$

$$\frac{\partial A}{\partial t} = \gamma_{A1} n_1 + \gamma_{A2} n_2 - \delta_A A + D_A \nabla^2 A. \tag{S35}$$

Similar to the results in the Main text, for infinitely fast inhibitor diffusion, A is spatially-uniform with a magnitude that is now dependent on the mean concentrations of both types of bacteria over the entire domain. If s_1 is the surface area fraction occupied by the type-1 strain, then $n_1^* = 0, n_2^* = 1 - \delta_2(1 + \alpha A)$ and $n_1^* = 1 - \frac{\delta_1}{\gamma_1}(1 + A), n_2^* = 0$ are the two local fixed points. This yields the self-consistency condition resulting in the relation between s_1 and A:

$$s_1 \gamma_{A1}(1 - \frac{\delta_1}{\gamma_1}(1 + A)) + (1 - s_1)\gamma_{A2}(1 - \delta_2(1 + \alpha A)) = \delta_A A, \tag{S36}$$

then

$$A = \frac{s_1\gamma_{A1}(1-\frac{\delta_1}{\gamma_1}) + (1-s_1)\gamma_{A2}(1-\delta_2)}{s_1\gamma_{A1}\frac{\delta_1}{\gamma_1} + (1-s_1)\gamma_{A2}\delta_2\alpha + \delta_A}. \tag{S37}$$

Stationary fronts for infinitely fast inhibitor diffusion. First, we derive the condition for stationary fronts for the generalized two-variable model with $\delta_1 \neq \delta_2$. Since A affects the growth rate of n_2 in the subsequent analysis, we also do not scale out the growth rate of n_2 and write it explicitly as γ_2. Consider the equations

$$\frac{\partial n_1}{\partial t} = \gamma_1 n_1(1-n_1-n_2) - \delta_1 n_1 - \kappa n_1 n_2 + \nabla^2 n_1, \tag{S38}$$

$$\frac{\partial n_2}{\partial t} = \gamma_2 n_2(1-n_1-n_2) - \delta_2 n_2 + \nabla^2 n_2. \tag{S39}$$

We assume that $\kappa = \epsilon K$, $\delta_1 = \epsilon\Delta_1$, $\delta_2 = \epsilon\Delta_2$ with $\epsilon \ll 1$, and again introduce new variables

$$N = \epsilon^{-1}(n_1+n_2-1), \quad \xi = n_1 - n_2. \tag{S40}$$

Conversely, $n_1 = (1+\epsilon N+\xi)/2, n_2 = (1+\epsilon N-\xi)/2$. In new variables and in the first order in ϵ,

$$\partial_t N = -\frac{N}{2}(\gamma_1+\gamma_2) - \frac{N}{2}(\gamma_1-\gamma_2)\xi - \frac{1}{2}(\Delta_1+\Delta_2) - \frac{\xi}{2}(\Delta_1-\Delta_2) - \frac{K}{4}(1-\xi^2) + \nabla^2 N, \tag{S41}$$

$$\epsilon^{-1}\partial_t \xi = -\frac{N}{2}(\gamma_1-\gamma_2) - \frac{N}{2}(\gamma_1+\gamma_2)\xi - \frac{1}{2}(\Delta_1+\Delta_2)\xi - \frac{1}{2}(\Delta_1-\Delta_2) - \frac{K}{4}(1-\xi^2) + \epsilon^{-1}\nabla^2\xi. \tag{S42}$$

The first equation describes fast relaxation toward the solution

$$N = -\frac{(\Delta_1+\Delta_2) + \xi(\Delta_1-\Delta_2) + \frac{K}{2}(1-\xi^2)}{\gamma_1+\gamma_2+\xi(\gamma_1-\gamma_2)}. \tag{S43}$$

Assuming that the fast initial relaxation has occurred, and N is slaved to ξ, we can substitute N from Eq. (S43) in Eq. (S42). Returning to the original parameters κ and $\delta_{1,2}$, after simple algebra we get a single reaction-diffusion equation for the slow dynamics of ξ,

$$\partial_t \xi = f(\xi) + \nabla^2\xi, \tag{S44}$$

where

$$f(\xi) = \frac{1-\xi^2}{1+\Gamma\xi}\left[\frac{\delta_1+\delta_2}{2}\Gamma - \frac{\delta_1-\delta_2}{2} + (\Gamma-1)(1-\xi)\frac{\kappa}{4}\right] \tag{S45}$$

with $\Gamma = (\gamma_1-\gamma_2)/(\gamma_1+\gamma_2)$. For small $\delta_{1,2}$ and κ, this equation describes slow front propagation. Function $f(\xi)$ has two roots $\xi_{1,2} = \pm 1$ corresponding to stable fixed points of Eq. (S44), and an intermediate root at $\frac{\delta_1+\delta_2}{2}\Gamma - \frac{\delta_1-\delta_2}{2} + (\Gamma-1)(1-\xi)\frac{\kappa}{4} = 0$ corresponding to an unstable fixed point. Maxwell rule states that a front solution of the 1-D reaction-diffusion equation (S44) connecting stable fixed points ξ_1 and ξ_2 is stationary if $\int_{\xi_1}^{\xi_2} f(\xi)d\xi = 0$.

For finite Γ, integration of the full function (S45) yields the following expression for κ at which the front is stationary,

$$\kappa = \frac{3(\gamma-1)^2(\gamma^2-1-2\gamma\ln\gamma)}{2\gamma^3+3\gamma^2-6\gamma+1-6\gamma^2\ln\gamma}\left(\frac{\delta_1+\delta_2}{2} - \frac{\delta_1-\delta_2}{2}\frac{\gamma+1}{\gamma-1}\right), \tag{S46}$$

where $\gamma = \gamma_1/\gamma_2$.

Returning to the three-variable model (Eqs. (S33)-(S35)), we notice that for spatially uniform A, the rescaled growth rates are $\gamma_1^* = \frac{\gamma_1}{1+A}$ and $\gamma_2^* = \frac{1}{1+\alpha A}$, and

$$\gamma = \frac{\gamma_1^*}{\gamma_2^*} = \gamma_1\frac{1+\alpha A}{1+A}. \tag{S47}$$

Thus, the fronts become stationary when A is equal to uniform A^* at which γ and κ satisfy Eq. (S46). This value of A^* corresponds to a particular area fraction s_1^* according to Eq. (S37). Thus, the union of the curves defined by Eq. (S46) together with Eqs. (S37) and (S47) when s_1 changes from 0 to 1, will yield the region for stationary fronts where we can expect emergence of patterns.

Stability of stationary fronts. Next we derive the condition for stability of stationary fronts with respect to their uniform displacement. If there is a small front displacement that changes s_1 with respect to s_1^* by a perturbation Δs_1, then the ratio of γ_1/γ_2 changes as well, by $\Delta\gamma = \frac{\partial\gamma}{\partial A}\frac{\partial A}{\partial s_1}\Delta s_1$. It is easy to see that the stationary front is stable if $\Delta s_1 \Delta\gamma < 0$, so for $s_1 > s_1^*$, $\gamma < \gamma^*$, the front moves in the direction that decreases s_1 back to s_1^*. In the opposite case, the front will move in the direction to further increase s_1, and n_1 will win. Thus, the condition for stable stationary fronts is

$$\frac{\partial\gamma}{\partial A}\frac{\partial A}{\partial s_1} = \gamma_1\frac{\alpha-1}{(1+A)^2}\frac{\gamma_{A1}\gamma_{A2}[\alpha\delta_2(1-\frac{\delta_1}{\gamma_1})-\frac{\delta_1}{\gamma_1}(1-\delta_2)]+[\gamma_{A1}(1-\frac{\delta_1}{\gamma_1})-\gamma_{A2}(1-\delta_2))]\delta_A}{[s_1\gamma_{A1}\frac{\delta_1}{\gamma_1}+(1-s_1)\gamma_{A2}\delta_2\alpha+\delta_A]^2} < 0. \tag{S48}$$

If $\delta_1, \delta_2, \gamma_{A1}, \gamma_{A2} \ll 1$, the condition can be simplified to

$$(\alpha-1)(\gamma_{A1}-\gamma_{A2}) < 0. \tag{S49}$$

This means if n_2 produces A faster than n_1 ($\gamma_{A2} > \gamma_{A1}$), for the stationary fronts to be stable, the growth inhibition of n_2 should be stronger ($\alpha > 1$) and vice versa. If $\alpha = 1$, then $\gamma = \gamma_1$ is a constant, and the front is only stationary on a single curve, as in the two-variable model without long-range inhibition.

One example of the region for stationary fronts and pattern formation is shown in Fig. S4.

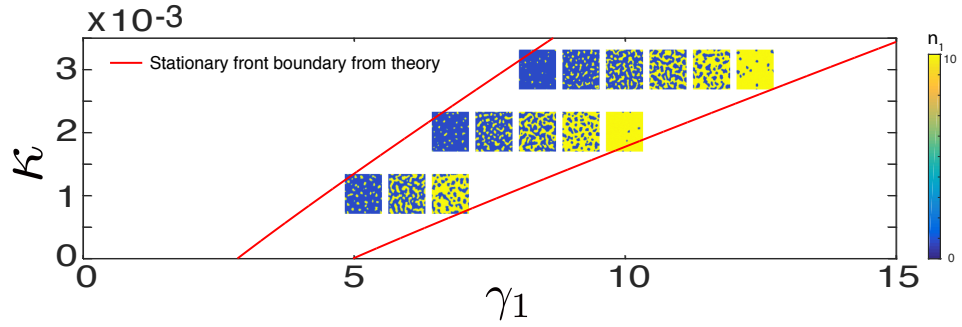

FIG. S4: Typical patterns emerging from random initial conditions in stochastic simulations of the dual-inhibition model for different values of parameters κ and γ_1. Other parameters are $n_0 = 10, \alpha = 0.1, \delta_1 = 0.01, \delta_2 = 0.005, \gamma_{A1} = 0.004, \gamma_{A2} = 0.001, \delta_A = 0.02, D_A = 12.5, P_n = 0.1$. The system size is 256×256.

IV. FRONT PINNING

To address the issue of possible front pinning due to spatial discretization of continuous reaction-diffusion-type models and compare the results with Blanchard et al.[1], we performed 1D simulations of front dynamics in the two-variable model (Eqs. (S3)(S4)), but changed the diffusion constant to a much smaller value $D_n = 0.01$ using different spatial discretizations of the computational domain of fixed length $L = 1024$. The results are shown in Fig. S9. The width of the wedge in the (γ_1, κ) plane in which fronts are stationary decreases exponentially with the number of grid points. When the number of spatial points is 1024, the width of the wedge is so small that it appears as a single line that is consistent with the continuum theory prediction (red curve). However, when the number of spatial points is reduced to 512, the wedge where fronts are stationary appears, which means front pinning. When the number of points is reduced even further, the region for front pinning becomes larger. The fewer number of grid points is equivalent to smaller diffusion constants for the same spatial resolution, thus these results also imply that, as the diffusion constant becomes smaller, the parameter region for pinned fronts increases, which is consistent with Ref. [1]. In our simulations, we used relatively high diffusion constant $D_n = 1$ and a sufficiently large number of grid points to make pinning effects negligible.

V. DETAILS OF THE DISCRETE LATTICE MODEL

In our stochastic simulations, we used a discrete lattice model to simulate strain competition and pattern formation. Specifically, the rules of the model are as follows: the number of cells in each strain is an integer number, so we used

unscaled parameters to carry out the simulations. We use a lattice model to do stochastic simulations, the rules for the simulations are:

1. We consider a square lattice model $0 \leq \{i, j\} \leq N$.

2. The number of individuals of each of the two species n_1, n_2 at each lattice site $\{i, j\}$ is integer, and the sum of $n_1(i, j)$ and$n_2(i, j)$ cannot exceed the maximum carrying capacity n_0.

3. The inhibitor A is defined as a real-valued field on the same lattice.

4. At each time step Δt, $n_1(i, j)$ can increase by one, $[n_1(i, j) \to n_1(i, j) + 1]$, with the probability $\gamma_1 n_1(i, j)[1 - (n_1(i, j) + n_2(i, j))/n_0]\Delta t$ or die $[n_1(i, j) \to n_1(i, j) - 1]$ with the probability $(\delta n_1(i, j) + \kappa n_1(i, j)n_2(i, j))\Delta t$. Similar probabilities apply to n_2 with swapping of subscripts $1 \leftrightarrow 2$ without the killing term.

5. Each cell can jump to one of four neighboring squares with the probability $P_n \Delta t$. The destination site is chosen at random, unless the neighboring site already has n_0 cells, then jumping there is forbidden.

6. We impose periodic boundary conditions in both dimensions for $n_1(i, j), n_2(i, j)$, and $A(i, j)$.

7. Reaction-diffusion dynamics of A is implemented via a split-step pseudo-spectral method.

VI. SUPPLEMENTARY MOVIES

Movie 1 Two-dimensional simulations of the deterministic continuum model with spatially uniform inhibitor A (infinite D_A) and random initial conditions. Parameters: $\gamma_1 = 4.5, \delta = 0.01, \kappa = 0.03, \gamma_A = 0.04, \delta_A = 0.02$.

Movie 2 Two-dimensional simulations of the deterministic continuum model with finite $D_A = 80$ and random initial conditions. Parameters: $\gamma_1 = 4.5, \delta = 0.01, \kappa = 0.03, \gamma_A = 0.04, \delta_A = 0.02$.

Movie 3 Two-dimensional stochastic simulations with random initial conditions. Parameters: $\gamma_1 = 3.5, \gamma_2 = 1, n_0 = 10, \delta = 0.01, \kappa = 0.003, \gamma_A = 0.004, \delta_A = 0.02, P_n = 0.1, D_A = 12.5$.

Movie 4 Two-dimensional stochastic simulations of dual-inhibition model with random initial conditions. Parameters: $\gamma_1 = 6, \gamma_2 = 1, n_0 = 10, \delta_1 = 0.01, \delta_2 = 0.005, \alpha = 0.1, \kappa = 0.001, \gamma_{A1} = 0.004, \gamma_{A2} = 0.001, \delta_A = 0.02, P_{n1} = 0.1, P_{n2} = 0.5, D_A = 12.5$.

[1] Andrew E Blanchard, Venhar Celik, and Ting Lu. Extinction, coexistence, and localized patterns of a bacterial population with contact-dependent inhibition. *BMC Systems Biology*, 8(1):1, 2014.

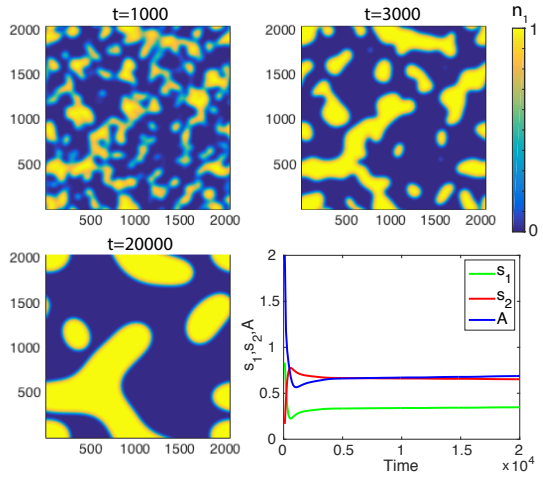

FIG. S5: Phase separation in the deterministic model with spatially uniform inhibitor A (infinite D_A) and random initial conditions. Three snapshots of n_1 and the time course of s_1, s_2 and A for 2D model. At large times, the area fractions s_1 and s_2 approach constant values, and the patterned state stabilizes. Parameters: $\gamma_1 = 4.5$, $\delta = 0.01$, $\kappa = 0.03$, $\gamma_A = 0.04$, $\delta_A = 0.02$.

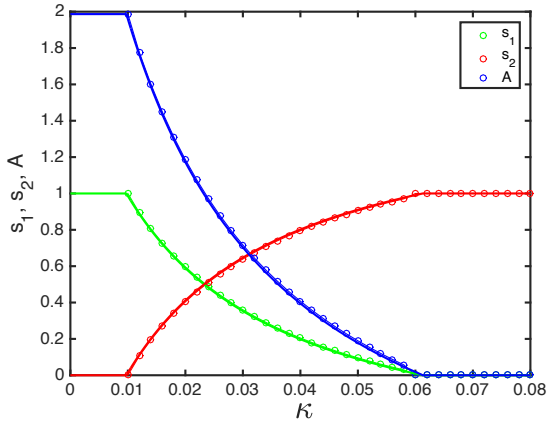

FIG. S6: Final area fractions of the two strains and the inhibitor level A as functions of the killing rate κ in the deterministic 1D model with spatially uniform inhibitor A (infinite D_A) and random initial conditions. The solid curves show the theoretical predictions using Eqs. (4)(6) in the Main text, and the circles show the simulation results. Parameters: $\gamma_1 = 4.5, \delta = 0.01, \gamma_A = 0.04, \delta_A = 0.02$, system size is 4096.

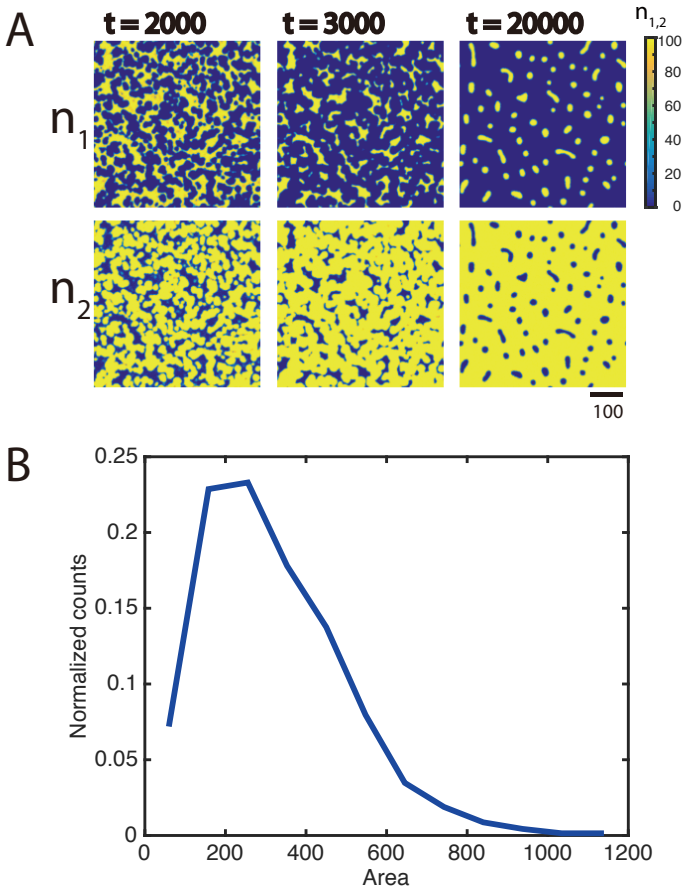

FIG. S7: Discrete stochastic simulations of pattern formation in a mixture of T6SS-sensitive (n_1) and T6SS-active (n_2) bacteria. (A) Three snapshots of a typical simulation. (B) Area distribution of spots of n_1 at $t = 20000$. The distribution result is from 10 stochastic simulations. Parameters: $\gamma_1 = 3, \gamma_2 = 1, n_0 = 100, \delta = 0.01, \gamma_A = 0.0001, \delta_A = 0.005, P_n = 0.04, D_A = 5$ and $\kappa = 0.00025$.

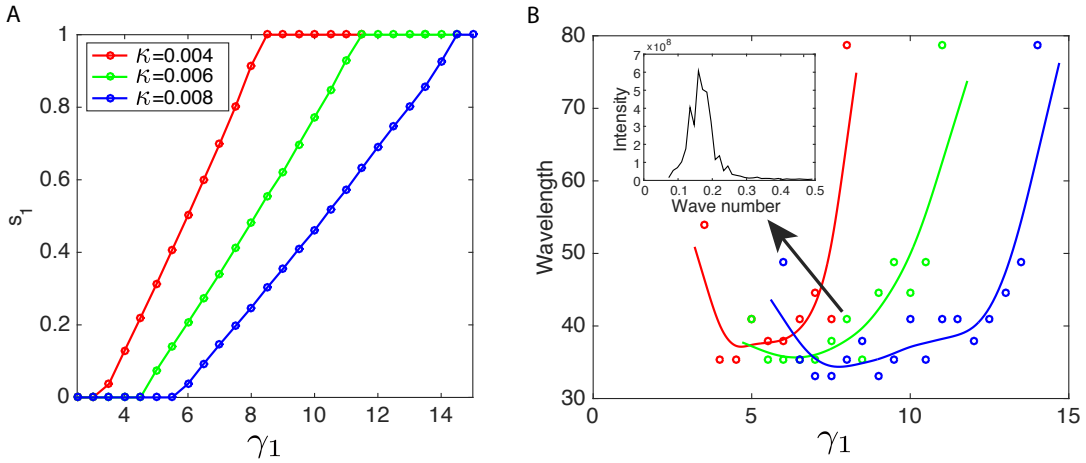

FIG. S8: Analysis of the patterns in stochastic simulations in Fig. 6. (A) n_1 area ratio s_1 vs. γ_1 in stochastic simulations for different κ. The fraction of n_1 changes continuously from 0 to 1 as the control parameter γ_1 moves across the pattern-forming range. (B) Peak wavelength of the asymptotic pattern vs. γ_1 for the same three values of κ as in panel (A). The circles are from simulations. The curves are smoothing spline extrapolated of the circles with the same color. The characteristic scale is diverging near the boundaries of the pattern-forming region in the parameter space. Inset: the power spectrum for $\kappa = 0.006, \gamma_1 = 8$. It has a well-defined peak corresponding to the characteristic distance between the spots or the period of the labyrinthine pattern.

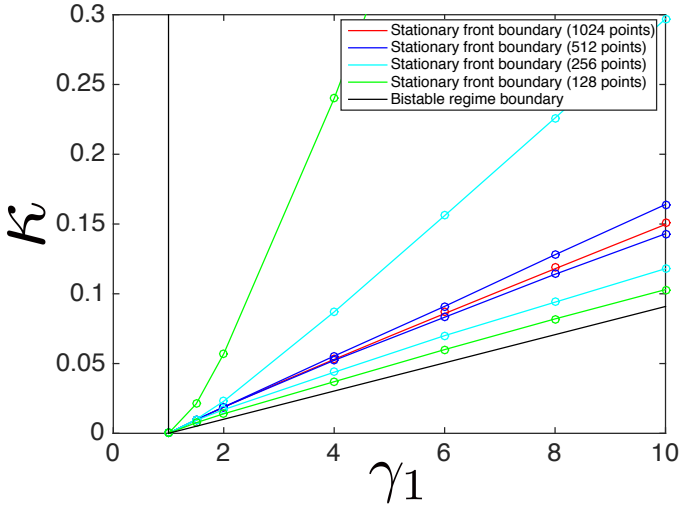

FIG. S9: Coarse spatial discretization leads to front pinning in finite-difference numerical simulations. Different lines show the simulation results for different numbers of grid points. Parameters: $\delta = 0.01, D_n = 0.01$.